Proceedings of the 2025 SICE Festival with Annual Conference
September 9-12, 2025, Chiang Mai, Thailand

Method for Estimating the Moment on a Needle During Surgery Using a Puncture Robot for Automatic Insertion

Takayuki Matsuno[1], Wataru Muramoto[2], Taichi Ozawa[2], Yuichiro Toda[1], Tetsuhi Kamegawa[1], Yusuke Matsui[3], Takao Hiraki[3]

[1] Faculty of Environmental, Life, Natural Science and Technology, Okayama University, Okayama, Japan
(E-mail: matsuno@okayama-u.ac.jp)
[2] Graduate school of Environmental, Life, Natural Science and Technology, Okayama University, Okayama, Japan
[3] Faculty of Medicine, Dentistry and Pharmaceutical Sciences, Okayama University, Okayama, Japan

Abstract: We have developed a CT-fluoroscopy-guided needle-puncture robot named Zerobot to assist in interventional radiology (IR) procedures. Currently, Zerobot is remotely operated by the surgeon using a controller. The next goal is to achieve automated needle insertion with Zerobot, which requires the integration of several techniques. In this study, we focus on estimating the bending moment applied to a puncture needle using CT images. In previous work, a method for automatically detecting needle puncture from a series of CT images was proposed. To obtain information on needle deflection and the forces acting on it, the curvature of candidate needle points in 3D space must be determined. We fit a polynomial curve through the thinned set of candidate points representing the needle path. Information derived from the fitted polynomial is then used to compute both the signed curvature and the corresponding bending moment.

Keywords: Interventional radiology, Automatic puncture, CT volume data, needle bending moment

1. INTRODUCTION

In recent years, the importance of medical care has been increasing due to social issues such as the declining birthrate and aging population. One surgical technique that has attracted particular attention is interventional radiology (IR), in which a needle or catheter is inserted into the body using diagnostic imaging techniques such as CT fluoroscopy and X-ray fluoroscopy, and treatment is performed percutaneously. CT fluoroscopy-guided needle puncture in IR has been applied to lung cancer treatment, liver cancer treatment, biopsy, and various other treatments. IR is less invasive than conventional surgery and can be performed under local anesthesia. Another advantage is the short hospitalization period, with many patients being discharged within three to four days after surgery. Currently, IR is performed manually by human operators. According to physicians, the target malignancy can be as small as 5 mm in diameter, so the surgeon must position the needle carefully and precisely. In addition, because the surgeon performs the procedure in close proximity to the CT gantry, there is concern that the surgeon may be exposed to radiation generated during fluoroscopy.

Although protective clothing and the use of forceps have been devised to prevent radiation exposure, they have not yet completely prevented radiation exposure. Therefore, robots such as Acubot [1], CTbot [2], MAXIO [3, 4], and INNOMOTION [5] have been developed to improve needle positioning accuracy and reduce radiation exposure to the surgeon. However, most of these robots are designed to assist physicians with guided puncture procedures. Zerobot, which is a remote-controllable needle-puncture robot developed by us, enables robotic IR for entire process positioning far from a CT scanner

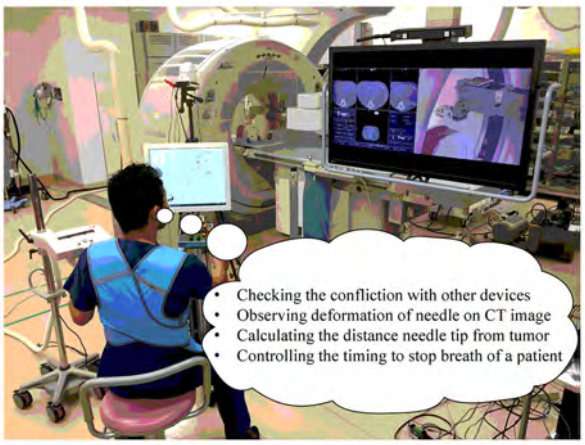

Fig. 1 Issue on surgeon during robotized surgery

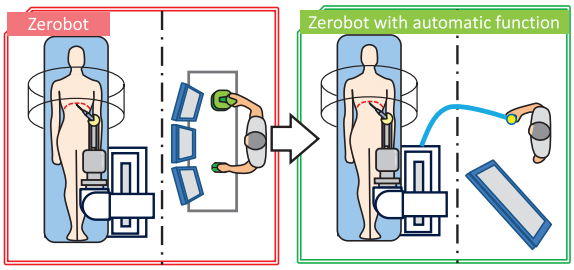

Fig. 2 Concept of automatic function on needle puncture robot

[6, 7]. We have conducted First-in-human examination with Zerobot in 2016 [8]. The remote-controlled procedure is, however, burdensome for the surgeon because the surgeon must simultaneously consider many factors like illustrated in Fig.1. For example, checking the conflict between a puncture robot and CT scanner, preventing large needle deformation while monitoring CT images, the direction of needle and distance toward the tu-

† Takayuki Matsuno is the presenter of this paper.

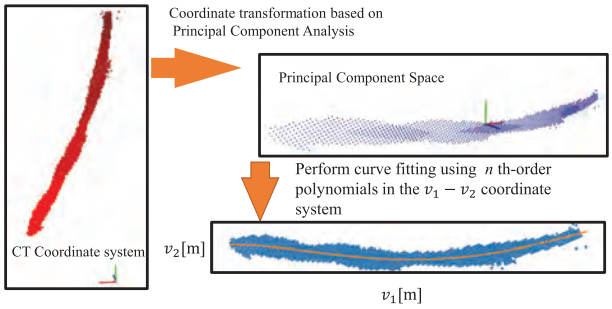

Fig. 3 Overview of bending moment estimation

mor for the control trajectory, and instructing the patient when to hold their breath, are actual tasks for the surgeon during the IR robot surgery. In addition, it requires training for doctors to achieve the fine accuracy of needle tip with robot controlling. Therefore, the next goal of teleoperation is automatic puncture. The concept of automatic puncture is depicted in Fig.2. In the automatic puncture, the surgeon orders only going or stopping to the robot through a wire that does not require the control interface. Automatic puncture requires the integration of several techniques, such as determination of the needle puncture route and avoidance of contact with peripheral devices, but information on the bending moment applied to the needle is necessary to prevent needle breakage. In this study, the method to estimate the bending moment of a puncture needle using CT volume data is proposed.

2. BENDING MOMENT ESTIMATION

2.1. Basis to calculate moment

For the goal of automatic needle insertion using a robot, information of the bending moment on the needle is necessary for preventing needle broken in the body of patients. Here, we propose a method to estimate the bending moment from the detected needle shape. In order to estimate the bending moment from the pixel data in CT volume data, Principal Component Analysis (PCA) is utilized to calculate the needle's principal axis direction. The transform matrix obtained from the principal component analysis projects the point data of needle candidate onto a new coordinate system with v_1, v_2, and v_3 as axes. Fig. 3 illustrates the projection of needle candidate points onto the v_1-v_3 coordinate system.

Next, the curved centerline passing through those points is calculated as a polynomial with respect to v_1 in both of the v_2 and v_3 directions, as equations (1) and (2).

$$v_2(v_1) = \sum_{i=0}^{n} a_i v_1^i \tag{1}$$

$$v_3(v_1) = \sum_{i=0}^{n} b_i v_1^i \tag{2}$$

Here, n is the order of polynomial to be determined by the designer. The coefficients a_i and $b_i (i = 0, 1, ..., n)$ are obtained by minimizing the squared error by fitting a polynomial of order n. Then, signed radius of curvature

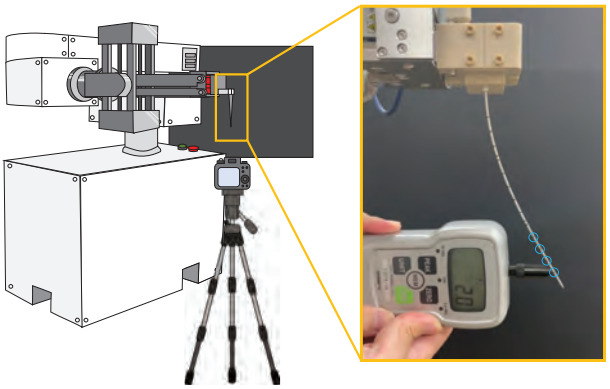

Fig. 4 Appearance of experiment for confirmation

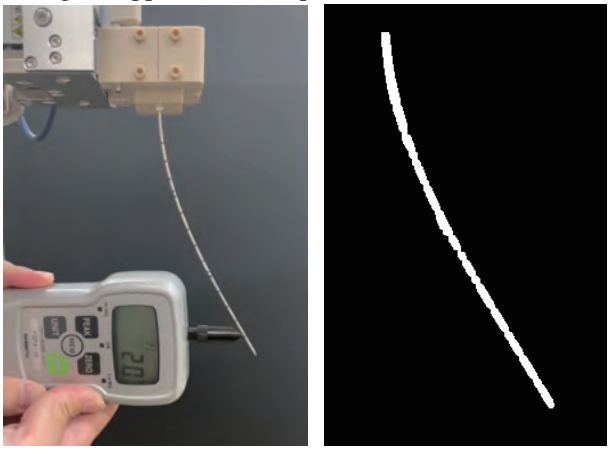

Fig. 5 Extracted needle form in confirmation experiment

$\hat{R}_{v2}$ of the center line on $v_1 - v_2$ plane is calculated as (3).

$$\hat{R}_{v2}(v_1) = \frac{\{1 + (v_2')^2\}^{3/2}}{v_2''} \tag{3}$$

$$v_2' = \frac{dv_2}{dv_1} = n a_n {v_1}^{n-1} + ... + a_1 \tag{4}$$

$$v_2'' = \frac{d^2 v_2}{d{v_1}^2} = n(n-1) a_n {v_1}^{n-2} + ... + 2a_2 \tag{5}$$

$\hat{R}_{v2}$ is derived from derivative v_2 by v_1, and it can be calculated with coefficients a_i. Finally, bending moment on the needle around v_3 axis M_{v3} is calculated as (6).

$$M_{v3}(v_1) = -\frac{EI}{\hat{R}_{v2}(v_1)} \tag{6}$$

Here, E is Young's modulus, which depends on the material of needle. I is Moment of inertia, which depends on the cross section form of needle. In addition, $M_{v2}(v_1) = \frac{EI}{\hat{R}_{v3}(v_1)}$ is also calculated in the same manner.

2.2. Experiment to confirm the process

To compare the results of the proposed method with theoretical values, an experiment was conducted in a simplified setting using a commercial camera instead of a CT scanner. The appearance of the simple experiment

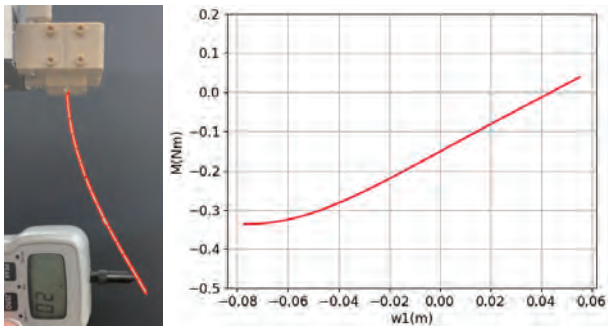

Fig. 6 Captured needle form and calculated moment around v_3 axis

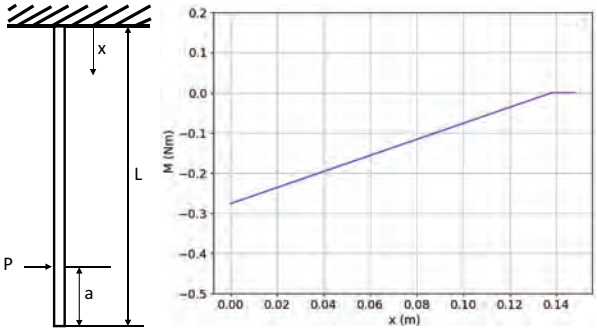

Fig. 7 Theoretical moment based on beam theory

is shown in Fig. 4. In this setup, the robot holds a biopsy guiding needle vertically, and the needle tip is pushed horizontally and parallel to the camera's imaging plane using a force gauge to measure the applied force. The form of needle was extracted as shown in Fig.5 based on contrast between the needle and background. The picture is rescaled based on the information that the needle length equals 150mm. Then, based on PCA analysis in 2D these pixels are projected into $v_1 - v_2$ plane under assumption $v_3 = 0$. After that, the moment is calculated with proposed method as shown in Fig. 6 with order $n = 3$. Here, it is assumed that $E = 200$GPa and $I = 5.20 \times 10^{-12}$ m^4. Those parameters are based on real biopsy guiding needle made of stainless iron. The theoretical moment in experimental situation based on beam theory, which is assuming small deformation, is plotted in Fig. 7. An equation to calculate moment is shown in Eq. (7).

$$M(x) = \begin{cases} -P(L-x) & (0 \le x \le L-a) \\ 0 & (L-1 < x \le L) \end{cases} \quad (7)$$

It can be confirmed that the moment calculated from captured image is almost the same as theoretical moment except near the tip of needle. Since a third-order polynomial cannot model branching or discontinuities, discrepancies appear near the needle tip in the estimated moment.

3. PIXEL DATA ON 3D SPACE

3.1. Overview

In previous research, a form of needle is identified in two-dimensional CT images [9]. Then, the next step is to estimate the needle deflection or stress from CT volume data for preventing needle broken during automatic puncture. So as to construct points of the needle in 3D space, each CT image should be projected into the space base on the elements of CT DICOM data, such as pixel spacing, slice width, and so on. This information is written in each DICOM files.

In experiment to confirm in previous section, deflection force is applied on the direction perpendicular to insertion. In the actual situation, the reaction force against insertion is also applied. In this situations, feasible order of polynomial expressing curvature is not known. Therefore order of polynomial n is compared in the range 2 to 7 with the evaluation of applied moment on needle.

3.2. Calculation of bending moment with CT images

To confirm whether bending moment on needle can be estimated from CT image series, M_3 is calculated from actual CT images. First, actual CT images are projected to 3D space considering pixel spacing factor. Then, points of the needle is projected with PCA method onto v_1 - v_3 space. Finally, each polynomial curve is fit with respect to minimize square mean errors for v_1 - v_2 plane. On the other hand, it was found that feasible curve can not be obtained in the v_1 - v_3 plane, since points on v_1 - v_3 plane have small deviation, Figure 8 shows the points of the needle in v_1 - v_2 plane and fit curve with order n of polynomial equals from 2 to 7. Also, estimated bending moment $M_3(v_1)$ for each order n is plotted on Fig. 9. In Fig.9, M_3 has various forms according to order of polynomial n, even though Fig.8 has almost same fiting curves in changing n. When n=6 or 7, M_3 make unstable or non-physical results that are not reliable as a beam form for external force. On the other hand in the case of n=2, M_3 becomes almost a straight line. It is a same result when assuming the needle form is arc shape. In those senses, order of polynomial n equals 3, 4 or 5 for expressing bending needle form. According to the previous experiment, M_3 will be zero near the tip of needle, when external force is applied to near the tip of needle without external moment. Such condition occurs a needle is straight inserted into the body. When n equals 3, M_3 almost equals zero at v_1=0.15m. Meanwhile M_3 almost is larger than zero at v_1=0.15m, when n = 4 or 5. This suggests that the polynomial curve make over-fitting to the points including noise. Also there is possibility to make the needle form S-curve, which cannot be expressed with n=3. Therefore, so as to improve the estimation accuracy, the method to reduce noise in points of the needle is proposed in next section. On the other hand, there is small distribution of points in v_3 direction as shown in Fig.10. It is clear that M_2 caused by curves in v_3 direction is very small and difficult to be estimated. Therefore, M_3 caused by curves in v_3 direction is focused on in this paper.

3.3. Thinning process for points of the needle

Due to the characteristics of the CT scanner, the needle candidate points are noisy and are detected as thicker than the actual needle. Therefore, thinning is necessary to make them closer to the actual needle shape. Principal Component Analysis is used to thin the points of needle in 3D space. Thinning process is performed for the bend-

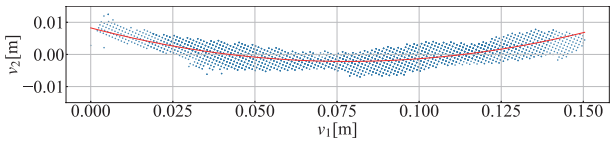

(a) n=2

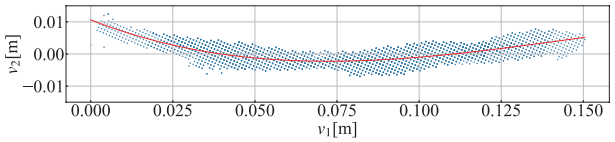

(b) n=3

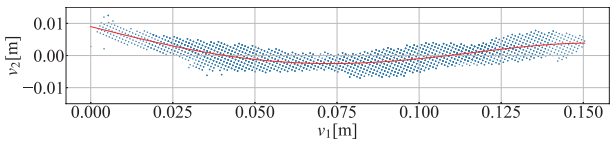

(c) n=4

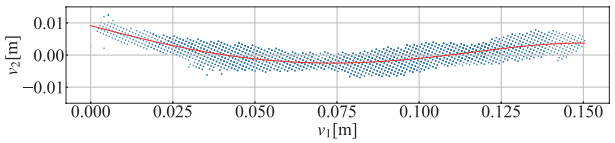

(d) n=5

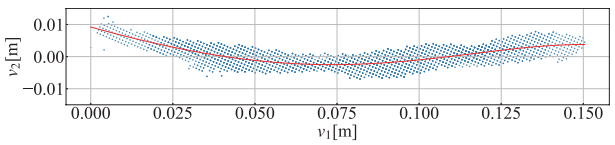

(e) n=6

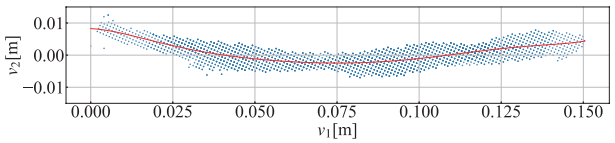

(f) n=7

Fig. 8 polynomial curve in v_1 - v_2 plane for the condition n= 2 to 7

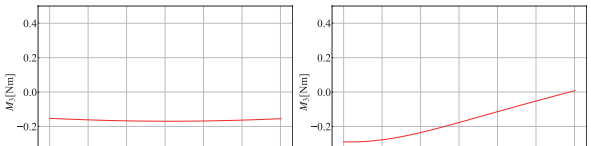

(a) n=2

(b) n=3

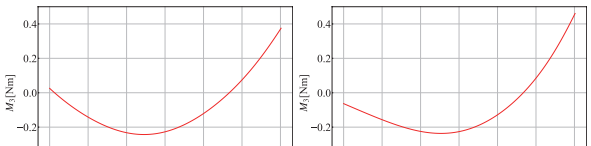

(c) n=4

(d) n=5

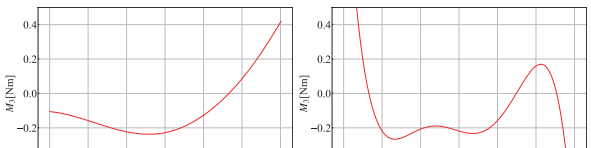

(e) n=6

(f) n=7

Fig. 9 M_3 for the condition n = 2 to 7

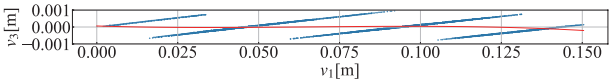

Fig. 10 third-order polynomial curve in v_1 - v_3 plane

ing curvature. The detail of thinning method is as below.

First, contour points in the volume data are extracted. The CT image series are individually converted into raster images, and contours are extracted using the OpenCV library. Both these points and the candidate needle points identified in previous research are projected from pixel coordinates to xyz coordinate system. The point clouds representing the puncture needle are visualized in the simulation space using the Open3D library [10]. The results of contour inspection of the volume data of the CT images on the same series are shown in Fig. 11. The red points on the image indicate the detected contour points. The results of contour extraction from the CT image volume data in the same series are presented in Fig. 12. The light red points in this image represent the detected contour points.

The point closest to the gripper of the needle in simulation space is selected. Then a sphere with a radius of 30 mm is created centered on this point, and the points inside the sphere are used as the first calculation object. Fig.13 shows a model representing the relation of points and the sphere. Principal Component analysis is performed on the points to be calculated to find the first principal component. The calculated first principal component represents the rough orientation of the needle to be calculated. After that, a cylinder with a radius of 0.8 mm, which is actual radius of the needle, is created with the calculated first principal component as its central axis. Points outside this cylinder are removed. With this procedure, only the points inside the cylinder remain, and the needle can be thinned in the first target segment. Figure 14 shows an overview of removing points outside of centerline using Principal Component Analysis. After thinning is completed in the first target segment, thinning continues for the next segment. In thinning in the next segment, the point closest to first sphere after first thinning is set as the center point of the second sphere. A calculation for second segment is similarly performed. Figure 15 shows a model representing the second calculation target segment. By repeating the above process from the base of the needle to the tip, segmented thinning using principal component analysis is performed on the entire needle.

3.4. Calculation of bending moment after thinning process

Figure 16 shows polynomial curve for the points of the needle after thinning process with order n of polynomial equals from 3 to 5. Estimated bending moments $M_3(v_1)$ based on those polynomial curve for each order n is plot-

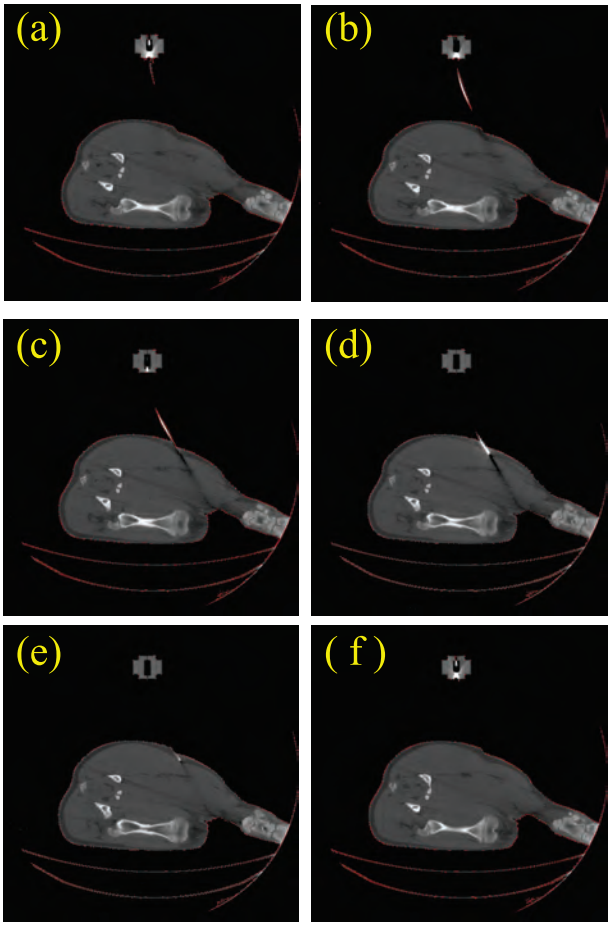

Fig. 11 Puncturing needle on CT images during puncture experiment with animal:red lines are contour to pickup surfaces of objects in 3D space

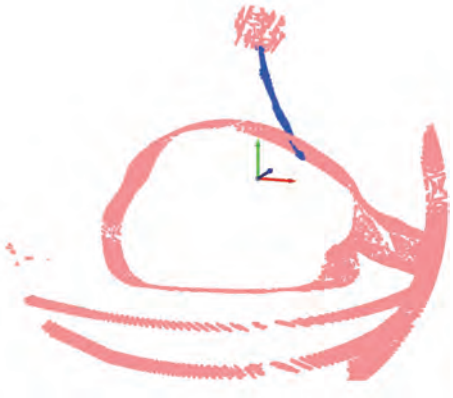

Fig. 12 Visualization of needle and body of animal in simulation space

ted on Fig. 17. Compared $M_3(v_1)$ in Fig.17 in the case of n = 4 or 5 with ones in Fig.9, the values around v_1 = 0.14[m] is close to zero. In this sense, noise reduction using Principal Component Analysis is effective for estimation of bending moment of the needle using CT volume data.

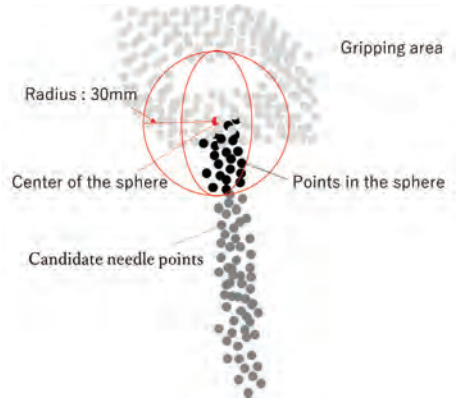

Fig. 13 First step of thinning process of needle form points

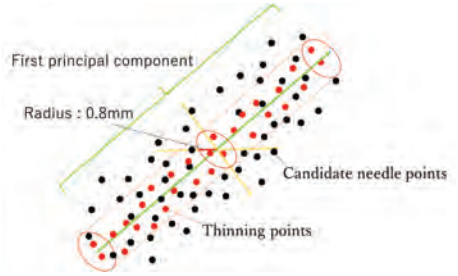

Fig. 14 Overview of methods for removing points

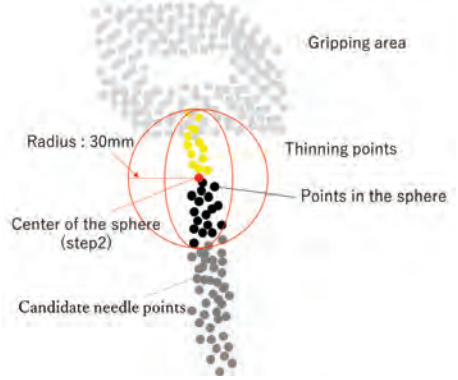

Fig. 15 Second step of thinning process of needle form points

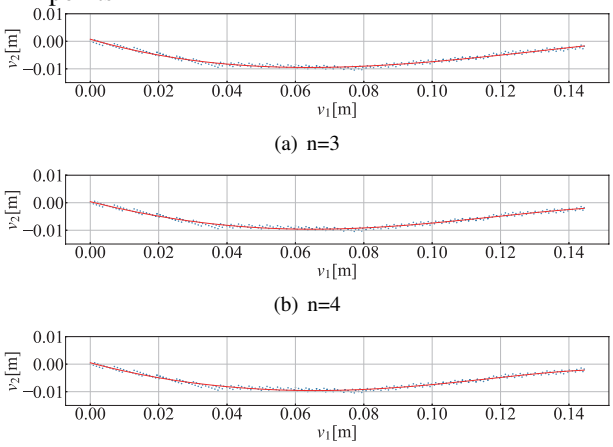

(a) n=3

(b) n=4

(c) n=5

Fig. 16 polynomial curve in v_1 - v_2 plane for the condition n=3 to 5: The needle points are thined to noise reduction

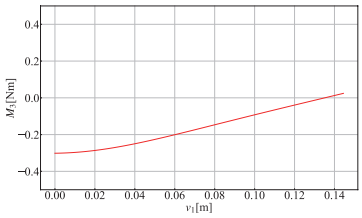

(a) n=3

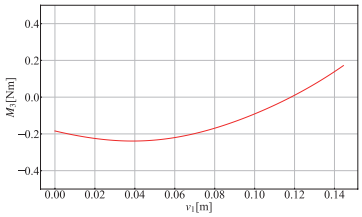

(b) n=4

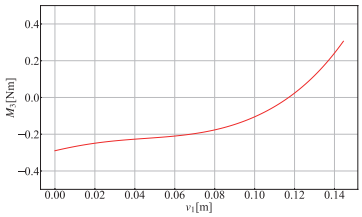

(c) n=5

Fig. 17 M_3 for the condition n=3 to 5 with noise reduction method

4. CONCLUSIONS

A method to obtain the bending moment applied to the needle during puncture is proposed. Polynomial approximation of the centerline passing through the detected needle points was conducted. Based on coefficients of those polynomial, bending moment of needle is estimated. Feasible order of polynomial is discussed based on the estimated bending moment M_3. Then, method to reduce noise of the needle points for the purpose of improvement in estimation of bending moment on the needle is proposed. The effectiveness is confirmed based on actual CT volume data.

ACKNOWLEDGMENT

This work was supported by JSPS KAKENHI Grant Number JP23K03758.

REFERENCES

[1] D. Staianovici, K. Cleary, A. Patriciu, D. Mazilu, A. Stanimir, N. Craciunoiu, V. Watson, and L. Kavoussi, "Acubot: A robot for radiological interventions," *IEEE TRANSACTIONS ON ROBOTICS AND AUTOMATION*, vol. 19, no. 5, pp. 927–930, 2003.

[2] B. Maurin, B. Bayle, O. Piccin, J. Gangloff, M. d. Mathelin, C. Doignon, P. Zanne, and A. Gangi, "A patient-mounted robotic platform for ct-scan guided procedures," *IEEE Transactions on Biomedical Engineering*, vol. 55, no. 10, pp. 2417–2425, 2008.

[3] Y. Koethe, S. Xu, G. Velusamy, B. J. Wood, and A. M. Venkatesan, "Accuracy and efficacy of percutaneous biopsy and ablation using robotic assistance under computed tomography guidance: a phantom study," *European Radiology*, vol. 24, pp. 723–730, Mar 2014.

[4] B. J. J. Abdullah, C. H. Yeong, K. L. Goh, B. K. Yoong, G. F. Ho, C. C. W. Yim, and A. Kulkarni, "Robotic-assisted thermal ablation of liver tumours," *European Radiology*, vol. 25, pp. 246–257, Jan 2015.

[5] A. Melzer, B. Gutmann, T. Remmele, R. Wolf, A. Lukoscheck, M. Bock, H. Bardenheuer, and H. Fischer, "Innomotion for percutaneous image-guided interventions," *IEEE Engineering in Medicine and Biology Magazine*, vol. 27, no. 3, pp. 66–73, 2008.

[6] T. Hiraki, T. Kamegawa, T. Matsuno, and S. Kanazawa, "Development of a robot for ct fluoroscopy-guided intervention: Free physicians from radiation," *Jpn., J. Incrvcnt Radiol*, vol. 29, pp. 375–381, 2014.

[7] T. Hiraki, T. Kamegawa, T. Matsuno, J. Sakurai, Y. Kirita, R. Matsuura, T. Yamaguchi, T. Sasaki, T. Mitsuhashi, T. Komaki, Y. Masaoka, Y. Matsui, H. Fujiwara, T. Iguchi, H. Gobara, and S. Kanazawa, "Robotically driven ct-guided needle insertion: Preliminary results in phantom and animal experiments," *Radiology*, vol. 285, no. 2, pp. 454–461, 2017. PMID: 28604237.

[8] T. Hiraki, T. Kamegawa, T. Matsuno, J. Sakurai, T. Komaki, T. Yamaguchi, K. Tomita, M. Uka, Y. Matsui, T. Iguchi, H. Gobara, and S. Kanazawa, "Robotic needle insertion during computed tomography fluoroscopy$2013guided biopsy: prospective first-in-human feasibility trial," *European Radiology*, vol. 30, pp. 927–933, Feb 2020.

[9] S. Kobayashi, Y. Toda, T. Matsuno, K. Mayumi, W. Muramoto, N. Fujitsuka, T. Tanaka, T. Kamegawa, and T. Hiraki, "Automatic detection of puncture needle from ct image with deep learning and difference of ct value along craniocaudal direction," in *2023 IEEE International Conference on Systems, Man, and Cybernetics (SMC)*, pp. 4947–4952, 2023.

[10] Q.-Y. Zhou, J. Park, and V. Koltun, "Open3D: A modern library for 3D data processing," *arXiv:1801.09847*, 2018.